

Placental Flattening via Volumetric Parameterization

S. Mazdak Abulnaga¹, Esra Abaci Turk², Mikhail Bessmeltsev³, P. Ellen Grant², Justin Solomon¹, and Polina Golland¹

¹ Computer Science and Artificial Intelligence Lab, MIT, Cambridge, MA, USA

² Fetal-Neonatal Neuroimaging and Developmental Science Center, Boston

Children’s Hospital, Harvard Medical School, Boston, MA, USA

³ Department of Computer Science and Operations Research, Universit de Montral, Montral, QC, Canada
abulnaga@mit.edu

Abstract. We present a volumetric mesh-based algorithm for flattening the placenta to a canonical template to enable effective visualization of local anatomy and function. Monitoring placental function *in vivo* promises to support pregnancy assessment and to improve care outcomes. We aim to alleviate visualization and interpretation challenges presented by the shape of the placenta when it is attached to the curved uterine wall. We flatten the volumetric mesh that captures placental shape to resemble the well-studied *ex vivo* shape. We formulate our method as a map from the *in vivo* shape to a flattened template that minimizes the symmetric Dirichlet energy density to control distortion throughout the volume. Local injectivity is enforced via constrained line search during gradient descent. We evaluate the proposed method on 28 placenta shapes extracted from MRI images in a study of placental function. We achieve sub-voxel accuracy in mapping the boundary of the placenta to the template while successfully controlling distortion throughout the volume. We illustrate how the resulting mapping of the placenta enhances visualization of the placental anatomy and function. Our code is freely available at <https://github.com/mabulnaga/placenta-flattening>.

1 Introduction

The placenta is a critical organ that connects the fetus to the maternal blood system [1]. Placental dysfunction increases the risk of pregnancy complications, with long-term effects on a child’s health and development and the mother’s health. It is therefore critical to monitor placental function and health *in vivo*. Ultrasound imaging and MRI capture detailed information about the placental position, shape, and tissue properties [17]. Blood oxygen level dependent (BOLD) MRI has recently been demonstrated to assess oxygen transport within the placenta [9, 17], providing initial evidence for clinical utility of MRI for functional assessment of the placenta. The use of in-utero anatomical and diffusion MRI [15] are also emerging areas of research. Compared with ultrasound, MRI

provides direct measurements of placental function in specific areas, providing signals necessary to study placental function and assess pathology [9,17].

The *in vivo* shape of the placenta is determined by the curved surface of the uterine wall to which it is attached during pregnancy. This presents significant challenges for interpretation of the MRI scans. No common standard exists for visualizing the functional or anatomical images of the placenta whose *in vivo* shape and location of attachment to the uterine wall vary greatly across subjects. We present a novel algorithm for mapping the placental shape observed in an MRI scan to a flattened template that resembles the organ's well-studied *ex vivo* flattened shape, to alleviate visualization challenges during *in vivo* examination and to facilitate clinical research and development of placental health biomarkers. Our work offers the first step towards developing a common coordinate system to enable statistical analysis.

We build on state-of-the-art mesh parameterization methods to represent and estimate the deformation of the placenta onto a template. Mesh parameterization is a topic of active research in geometric processing for mapping surfaces to canonical domains such as planes or spheres [5] while guaranteeing desirable properties of the mapping such as injectivity [12, 16]. When applied to cortical mapping, this parameterization facilitates visualization and population studies [3,8,18,19]. The formulation might seek a conformal mapping to a sphere [8], estimate the optimal map by minimizing a cost function that penalizes areal distortion [19], changes in the geodesic distances along the surface [3], or more commonly a combination of different measures of distortion [18].

The problem of placental parameterization is different from cortical mapping in two significant ways. Most importantly, unlike the inherently two-dimensional (2D) cortex, the placenta is a fully three-dimensional (3D) organ. Image information along the depth direction from the maternal to the fetal sides of the placenta is important for characterizing its function. The parameterization must therefore map the entire volume of the placenta, rather than only its boundary surface. Moreover, the shape of the placenta, while highly variable, is dramatically simpler than that of the cortex, promising efficient implementations that can be readily integrated into the clinical workflow.

In placenta imaging, a method for placental flattening has been recently demonstrated [10]. Their algorithm represents the placenta as a stack of parallel surfaces spanning the thickness of the organ. Each surface is flattened separately by mapping the boundary to a disk with each interior vertex moved to the average of its neighbors. In contrast, we propose a continuous volumetric mapping that ensures uniform consistency of the mapping throughout the volume and enables explicit control of the distortion in the resulting deformation.

Our algorithm estimates the transformation of the volumetric mesh to a template as a solution of an optimization problem. This formulation readily accepts a broad family of templates and shape distortion functions. In this paper, we choose two parallel planes as the template and minimize the symmetric Dirichlet energy [13] to penalize local deformations of the mesh. Our implementation takes advantage of GPU computing to parallelize gradient computation during the op-

timization, delivering an efficient implementation. We evaluate our method on images from an MRI study, demonstrating effective mapping of the highly variable placental shape to the template with minimal distortion and illustrate the promise of our algorithm to support clinical use of MRI in placental imaging.

2 Methods

We represent the placental shape as a tetrahedral mesh that contains N vertices, of which the first M vertices lie on the boundary, and K tetrahedra. In our experiments, we extract such meshes from segmented MRI scans as described later in the paper. We parameterize the mapping via mesh vertex locations in the template coordinate system and interpolate the deformation to the interior of each tetrahedron using a locally affine model.

2.1 Problem Formulation

Let $X \in \mathbb{R}^{3 \times N}$ be a matrix whose columns are the 3D coordinates of all mesh vertices in the template space with the boundary vertices forming the first M columns, and $X_k \in \mathbb{R}^{3 \times 4}$ be a matrix whose columns are the 3D coordinates of the four corner vertices of tetrahedron k ($k = 1, \dots, K$) in the template space. We use $Z_k \in \mathbb{R}^{3 \times 4}$ to denote a matrix whose columns are the 3D coordinates of the four corner vertices of tetrahedron k in the original image space. We further define B to be a 4×3 matrix that extracts three basis vectors defining the tetrahedron; the vectors originate from the first corner vertex of the tetrahedron and point to its other three corner vertices. The Jacobian matrix

$$J(X_k) = (X_k B) (Z_k B)^{-1} \quad (1)$$

captures the linear transformation of tetrahedron k based on the new vertex coordinates X_k in the transformed space while ignoring the translation component shared by its vertices.

We measure local distortion of the mapping using the symmetric Dirichlet energy density

$$\mathcal{D}(J) = \|J\|_F^2 + \|J^{-1}\|_F^2 = \sum_{i=1}^3 (\sigma_i^2 + \sigma_i^{-2}), \quad (2)$$

where $\|\cdot\|_F$ is the Frobenius norm and $\{\sigma_1, \sigma_2, \sigma_3\}$ are the singular values of matrix J [12, 13, 16]. We chose the symmetric Dirichlet energy as it penalizes expansion and shrinking equally and prevents tetrahedra from expanding or shrinking dramatically since the corresponding singular values or their reciprocals become unbounded. This distortion energy also favors a locally injective mapping by preventing tetrahedra from collapsing to a point.

Our mapping is formulated as an optimization problem over the mesh vertices that seeks to minimize

$$\phi(X) = \underbrace{\sum_{m=1}^M A_m T(x_m)}_{\text{Template match}} + \lambda \underbrace{\sum_{k=1}^K V_k \mathcal{D}(J(X_k))}_{\text{Distortion}}, \quad (3)$$

where $\{x_m\}_{m=1}^M$ are the boundary vertex coordinates in the template system, $T(\cdot)$ is a measure of distance from the template shape, A_m is the normalized barycentric area associated with vertex m on the boundary of the mesh (i.e., A_m is proportional to the sum of the areas of the faces that include vertex m and $\sum_{m=1}^M A_m = 1$), V_k is the normalized volume of tetrahedron k in the original shape space ($\sum_{k=1}^K V_k = 1$), and λ is a parameter that governs the trade-off between the template fit and the shape distortion. The formulation of the distortion term naturally accepts a range of distortion metrics provided they are differentiable in X . The distortion term regularizes the mapping.

2.2 Template

We define our template to be two parallel planes, one corresponding to the fetal side of the boundary, and the other to the maternal side. Function $T(\cdot)$ measures the distance to the appropriate plane:

$$T(x) = \begin{cases} (x^{(3)} - h)^2 & \text{if } x \in \mathcal{F}(\partial Z), \\ (x^{(3)} + h)^2 & \text{if } x \in \mathcal{M}(\partial Z), \\ 0 & \text{otherwise,} \end{cases} \quad (4)$$

where $x^{(3)}$ refers to the third coordinate of point x in the template coordinate system, ∂Z denotes the boundary of the mesh in the original image space, and $\mathcal{F}(\partial Z)$, $\mathcal{M}(\partial Z)$ denote the fetal and maternal sides of ∂Z . We use the term *rim* to denote the region of high curvature with a finite number of vertices that separates the fetal and maternal sides of the placenta. The rim is not mapped to either plane; the rim vertices are driven only by the distortion term. We investigated mapping to ellipsoid and cylinder templates, and present here the choice that led to the smallest distortion and yielded physiologically plausible visualization.

Placenta Boundary Parcellation. The template term (4) requires identifying the maternal and fetal sides of the placenta boundary. Since we expect the boundary normals to cluster into two distinct groups that correspond to the two sides of the placenta, we construct a metric of the boundary vertex similarity based on the angle between boundary vertex normals and project the vertices to a 1D space using spectral embedding [11].

For boundary vertex m , we determine the unit-vector normal \hat{n}_m as a weighted average over the mesh boundary triangles that contain vertex m , normalized to

have unit length. The weighting is proportional to the triangle areas. We construct an affinity matrix $W \in \mathbb{R}_+^{M \times M}$ whose (i, j) element $w_{i,j} = \exp \{ \gamma (\hat{n}_i^\top \hat{n}_j) \}$ for any two boundary vertices i and j that are connected by 3 or fewer edges (the three-ring neighborhood), and 0 otherwise. The parameter γ penalizes the local effect of variation in the orientation of the normals. The Laplacian of W is defined as

$$L = I - D^{-\frac{1}{2}} W D^{-\frac{1}{2}}, \quad (5)$$

where D is a diagonal matrix with $d_{i,i} = \sum_j w_{i,j}$ and I is the identity matrix. The second smallest eigenvector of L defines the spectral embedding of the boundary vertices that can be thresholded to segment the boundary into two components with consistent orientation of the normals [11]. The maternal side of the placenta boundary has a more convex shape due to its attachment to the uterine wall. We construct the convex hull of the boundary to assign the maternal label to the cluster with the larger number of vertices on the hull.

We define the rim of the placenta as the connected region separating the fetal and maternal sides. We identify vertices on the boundary of the two clusters, i.e., those with neighbors in the other cluster, and assign them to the rim. We approximate geodesic distance using Dijkstra's shortest path algorithm on mesh edges to define this neighborhood. Using the geodesic distance accounts for irregularities in the mesh and ensures the rim separates the two sides of the placenta with consistent width.

Since the rim is the region of highest curvature, a mean curvature-based clustering method would be another way to determine the three regions. In our experiments, we found the sensitivity of the mean curvature measure and irregularities in the mesh require considerable smoothing to obtain the three distinct connected components. Excessive smoothing distorts the mesh, resulting in an over-estimated rim and challenges in clustering placentae with less curved volumes.

2.3 Optimization

We minimize cost function $\phi(\cdot)$ in (3) using gradient descent. We initialize the mapping using the identity transformation. The gradient of the template term is linear in the vertices, $\frac{\partial T(x)}{\partial x^{(3)}} = 2(x^{(3)} \pm h)$. We derive the gradient of the symmetric Dirichlet energy term defined in (2) using the chain rule for matrices:

$$\begin{aligned} \frac{d \|J(X_k)\|_F^2}{d X_k} &= X_k \left[2B (Z_k B)^{-1} (Z_k B)^{-T} B^T \right], \\ \frac{d \|J(X_k)^{-1}\|_F^2}{d X_k} &= -2X_k B (B^T X_k^T X_k B)^{-1} B^T Z_k^T Z_k B (B^T X_k^T X_k B)^{-1} B^T. \end{aligned}$$

We employ line search to prevent tetrahedra from “flipping”, i.e., from crossing the singularity point of zero volume thereby enforcing local injectivity [16]. In every iteration, we determine the largest value η such that adjusting the current vertex locations X by $-\eta \nabla \phi(X)$ avoids singularities for all tetrahedra. The

(signed) volume V_k of tetrahedron k

$$V_k(\eta) = \frac{1}{6} \det((X_k - \eta \nabla \phi(X_k)) B), \quad (6)$$

is a cubic polynomial of η whose real and positive roots are the singularity points. The upper limit for η in line search is found by finding the smallest, positive, real root of (6) over all tetrahedra.

2.4 Intensity Mapping

Once the optimal vertex coordinates are determined by minimizing (3), we map image values inside the placenta to the template coordinate system. We use barycentric coordinates to determine the transformation for any given point inside the placenta. Specifically, any point x inside tetrahedron k can be represented as a linear combination of the tetrahedron's corner vertices through the point's barycentric coordinates $\alpha \in \mathbb{R}^4$, i.e., $x = X_k \alpha$, where $\alpha_i \geq 0$ for $i = 1, \dots, 4$, and $\sum_{i=1}^4 \alpha_i = 1$ [4]. Barycentric coordinates α_2 , α_3 , and α_4 can be computed from the point's Cartesian coordinates x as follows:

$$[\alpha_2 \ \alpha_3 \ \alpha_4]^T = (X_k B)^{-T} (x - X_k^1), \quad (7)$$

where X_k^1 is the first column of matrix X_k . Setting $\alpha_1 = 1 - (\alpha_2 + \alpha_3 + \alpha_4)$ completes the vector.

For each tetrahedron in the mesh, we identify voxels in the template coordinate space that are contained by the tetrahedron. Since our mapping is locally injective and affine, we use the voxel's barycentric coordinates $\{\alpha\}$ and the tetrahedron's original coordinates Z_k to compute the Cartesian coordinate of the voxel in the original image. We use the computed Cartesian coordinates to pull the image intensity into the template coordinate system using linear interpolation.

2.5 Implementation Details

We generate tetrahedral meshes from segmentation labelmaps using iso2mesh [2], a MATLAB-based toolbox that provides an interface to TetGen [14], a commonly used tetrahedral meshing library. Prior to applying the mapping, we center the original mesh and rotate it to align its principal axes to the axes of the template. We assume the algorithm converges when the Frobenius norm of the gradient is lower than 5×10^{-5} .

We implemented the algorithm in MATLAB using GPU functionality to parallelize the computation of the gradient and the line search. We ran our experiments on an NVIDIA Titan Xp (12GB) GPU. Each iteration took approximately 0.1 seconds to complete and ran for an average of 4083 iterations. The algorithm converged in less than twenty minutes for each subject in the study.

3 Experiments

Data: We illustrate the utility of the proposed approach on a set of 28 MRI scans from two studies. The first is a twin study that included seven pregnant women (gestational age: 28–34 weeks). All twin pregnancies had one placenta shared by the two twins. The second is a singleton pregnancy study that acquired MRI scans on eleven women (gestational age: 27 – 40 weeks). For 10 of these 11 subjects, scans were acquired lying in the supine and left lateral positions, yielding 20 total segmentations since the shape of the placenta differed across position. MRI BOLD scans were acquired on a 3T Skyra Siemens scanner (single-shot GRE-EPI, 3 mm isotropic voxels, interleaved slice acquisition, TR=5.8–8s, TE=32–36ms, FA= 90°) using 18-channel body and 12-channel spine receive arrays. The placenta was manually segmented, and the resulting segmentation label maps served as an input to the meshing software. The resulting meshes had an average of 6,500 tetrahedra and 2,800 surface triangles.

Parameters: We used a parameter sweep to determine the values of the hyper-parameters. We set shape distortion parameter $\lambda = 1$ as it was in the optimal trade-off range between the template matching and distortion (Fig. 1). We set the template half-height h to be half of the placenta thickness estimated from the histogram of the distance transform values inside the segmentation boundary. We set the spectral clustering parameter $\gamma = 20$, but found it worked robustly for $\gamma \in [20, 80]$. We used a boundary geodesic distance of 5 voxels as the width of the rim.

Evaluation: We visually assess the quality of the transformation by mapping the BOLD MRI intensity patterns to the template coordinate system. We examine the flattened mesh and the mapped BOLD MRI signal. We use the log-determinant of the Jacobian matrix $\log_2 \det(J(X_k))$ of tetrahedron k to quantify local volumetric distortion [7] and examine maps and distributions of distortion. We quantify metric distortion using the ratio of edge length $\log_2(x_{ij}/z_{ij})$, where edge z_{ij} is the length of edge (i, j) in the original mesh, and x_{ij} is the length of the same edge in the flattened mesh. Finally, we examine the shape distortion term in (3) to quantify the overall amount of distortion.

We compare our method with the prior parameterization approach in [10] where 2D surfaces spanning the placenta were independently parameterized to a disk in \mathbb{R}^2 . The surfaces were derived by cutting Euclidean level sets to minimize local curvature changes. To emulate their method, we derive such 2D surfaces by intersecting the flattened placenta volume with planes spaced one voxel apart, yielding a set of parameterized surfaces. These surfaces are then mapped to the original placenta volume using barycentric coordinates, yielding a set of surfaces the placenta. We use harmonic parameterization [6] to map each surface to a disk. A corresponding point

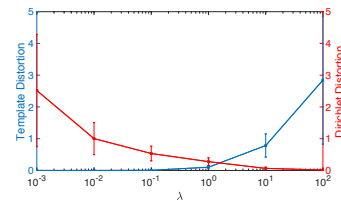


Fig. 1. The final template matching term and symmetric Dirichlet energy as a function of λ . The competing terms approach the optimal trade-off point near $\lambda = 1$.

in each surface is mapped to the north point of the disk. We scale the areas and edge lengths in the parameterized space to have 0–mean log areal and metric distortion, respectively.

3.1 Results

For all subjects in the study, our algorithm achieves sub-voxel accuracy of matching the template (median of 0.09 voxels, max. of 0.30 voxels). The symmetric Dirichlet energy is minimized by the identity transformation. The resulting transformations achieve close to minimum values of the symmetric Dirichlet energy (median is 3.87% higher than the smallest possible value, maximum is 9.04% higher than the smallest possible value).

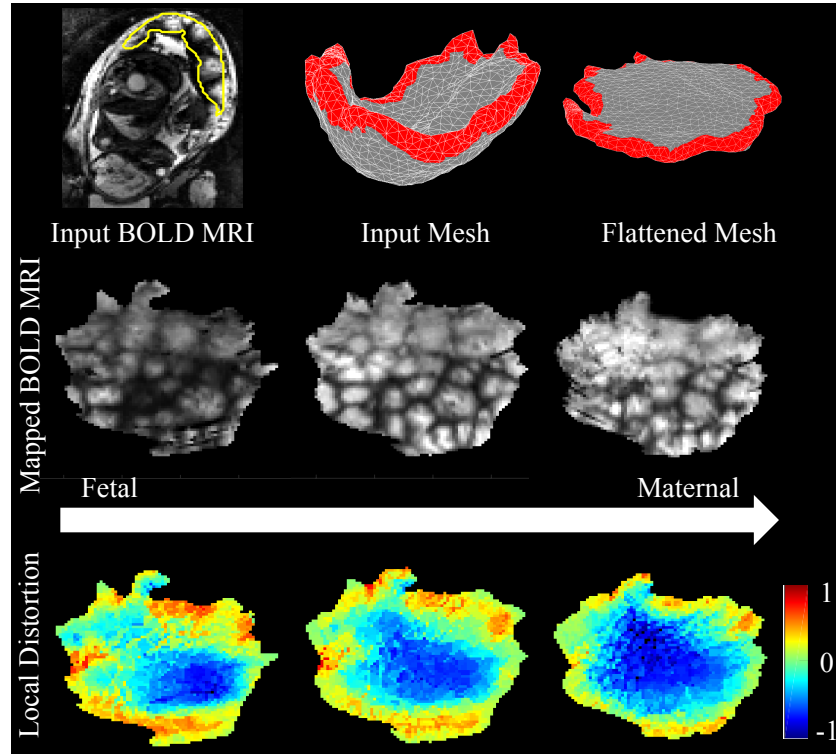


Fig. 2. Example twin pregnancy subject from the study. First row, left to right: segmentation of the placenta (yellow boundary) in an axial slice of the BOLD MRI volume, tetrahedral mesh of the original placenta with the placental rim in red, resulting flattened mesh. Second row: three sequential slices through the volume of the flattened mesh. The cotyledons, characterized by a honeycomb structure of small hyperintense regions, are immediately apparent in the flattened images. Third row: local distortion ($\log_2 \det(J(X_k))$) maps of the slices shown in the second row.

Fig. 2 illustrates the mapping results for one twin pregnancy placenta from the study. The mapped BOLD intensity patterns clearly visualize local anatomy and function as is apparent in the honeycomb structure of the cotyledons, which are the circular structures that exchange oxygen and nutrients between the surrounding maternal blood and the fetal blood in the chorionic villi [1]. Cotyledons appear hyperintense in BOLD MRI. We gain contextual information about the cotyledon distribution across the placenta and observe the enhanced regions at this particular time point in the BOLD MRI time series. The flattened view provides spatial information relevant for assessing placental function [9]. Furthermore, we observe limited volumetric distortion. Our approach enables more intuitive visualization of complex spatiotemporal signals, which in turn presents the opportunity to develop biomarkers to quantify regional signal variations in the organ.

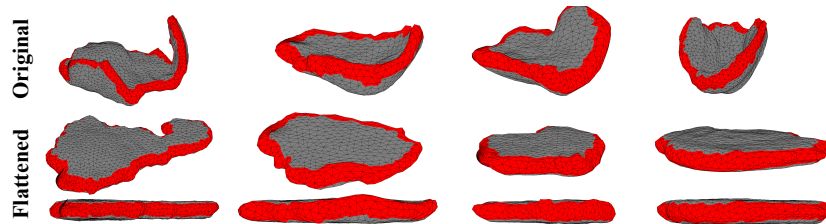


Fig. 3. Flattening results for four tetrahedral meshes of placentae from the study: one twin (left) and three singleton pregnancies. The region in red is the placental rim and the fetal sides are facing upwards. The greatly differing shapes in the dataset are robustly mapped. The estimated rim region is a faithful representation of the curved area separating the fetal and maternal sides.

Fig. 3 illustrates the mapping results for four placentae, highlighting the variability in shape encountered in the dataset. The algorithm maps difficult structures robustly, for example the fold in the first placenta and the bowl shape in the last. Fig. 3 also presents the estimated placental rim. We observe a fully connected component that effectively separates the three regions, highlighting the effectiveness of spectral clustering in separating the placenta boundary into its fetal and maternal components.

Fig. 4 demonstrates enhanced visualization of a real anatomical landmark (a cotyledon) and a fabricated one consisting of the letters “MIT” in the flattened space versus the *in vivo* volume. The flattened space is the inherent geometry of the placenta, and the letters could represent key landmarks or a spatial biomarker revealing pathology. We note that a cotyledon is clearly seen in the flattened view and is less easy to identify in the original volume. The curved geometry of the *in vivo* placenta demonstrates immediate difficulty in visualizing the details that are clearly seen in the flattened view, since contextual information is lost. Several

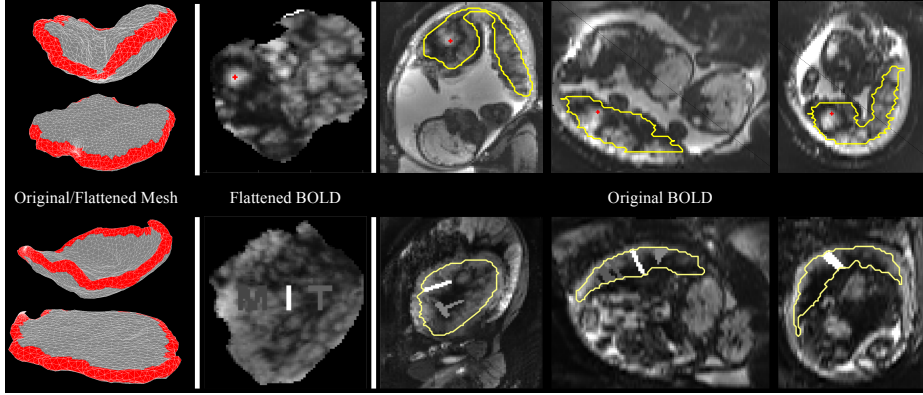


Fig. 4. Visual assessment a cotyledon structure (top) and a fabricated landmark, “MIT” (bottom) of two twin pregnancy subjects. Left to right: the original and flattened tetrahedral meshes; one slice of the flattened volume; three orthogonal cross-sections of the original volume. Segmentation of the placenta is outlined in yellow. Top image: the red marker indicates the approximate center of the cotyledon. The natural anatomical pattern of the cotyledon structure is immediately apparent in the flattened image. Bottom row: the landmark “MIT” is distributed axially throughout the flattened volume. Focusing on the center of the letter “I”, outlines can be made out in the original volume, but the context of the other letters is completely lost. Local anatomy is difficult to examine in the original volume due to the curved geometry of the uterine wall that determines the *in vivo* shape of the placenta.

views in the original image space are required to identify anatomical landmarks and obtain contextual information.

Fig. 5 presents statistical distributions of volumetric and metric distortions. We report statistics of the tetrahedra of all 28 placentae, and of mean distortion values across the 28 cases. For all subjects, the distortions are unimodal and have low variance as they are well-contained at the extrema. We also did not observe differences in distortion across twin and singleton pregnancies.

Fig. 5. Distributions of distortion. We report (i) the statistics of volumetric and metric distortion across all tetrahedra (All), weighted by tetrahedral volume in the original image space, and (ii) of the mean distortion values across the 28 cases (Mean). The distributions are unimodal and well-contained at the extrema.

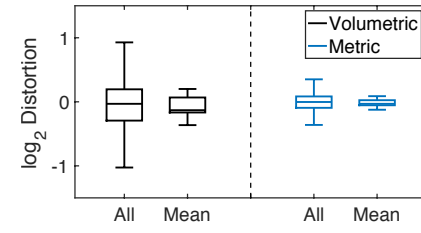


Fig. 6 compares our method with the baseline 2D approach. Our method produces considerably lower distortion across all subjects and the spatial dis-

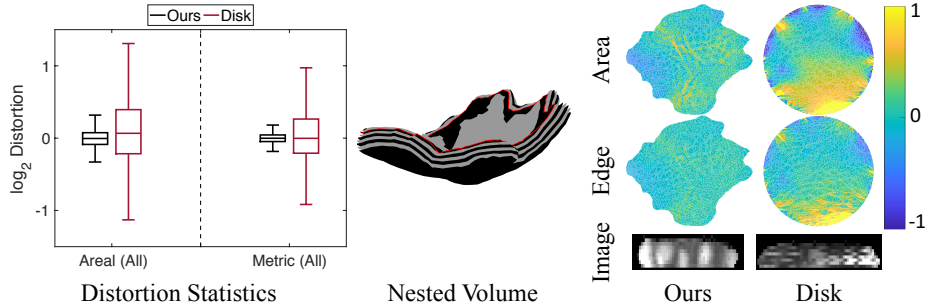


Fig. 6. Comparison of our method with the baseline 2D parameterization approach. Left: distributions of areal and metric distortion across all triangles (“All” in Fig. 5), weighted by triangle area in the original space. Middle: the nested volume shown is generated by stacking the sliced surfaces in the original image space. Alternating colors indicate consecutive surfaces, and the surface outlined in red is used to visualize distortion. Right: spatial distributions of distortion. Our method results in consistently lower distortion across all 28 cases. For each surface, distortions are distributed more homogeneously. Finally, the through-volume view of the mapped image intensity shows artifacts resulting from a lack of coupling across slices when parameterizing to a fixed boundary.

tributions of distortion are narrower with lower variance for our method. The harmonic mapping produces high distortion near the boundary and introduces misalignment of the flattened planes. Lack of coupling across planes produce imaging artifacts as seen in the cross-sectional view of the mapped image intensity. As expected, mapping to a fixed boundary results in greater distortion than our method. A free boundary approach is likely to produce lower distortion than mapping to a disk, though distortions resulting from lack of coupling across planes would persist. Similarly, properly aligning parameterized surfaces would introduce additional distortion. These results confirm the need for a volumetric parameterization method. Finally, we note that the nested surfaces in the original space were derived from the volumetric parameterization to the flattened space. In practice, estimating these surfaces is challenging and require a multi-step specialized pipeline as in [10].

4 Conclusion

In this work we developed a volumetric mesh-based mapping of the placenta to a flattened template represented by two parallel planes, resembling the *ex vivo* flattened shape of the organ, thereby enabling visualization of local anatomy and function. An immediate next step is to assess the utility for clinical research by quantifying the improvement in identifying known key biomarkers and anatomical features. We plan to extend the image mapping to similarly flatten regions outside the placenta to gain contextual information and visualize important anatomy such as the umbilical cord. In future work, we will improve

the template using anatomical data such as the umbilical cord insertion. The cord cannot be assumed to be inserted in the center of the placenta, especially for twin cases, and must be identified in the image. We are currently collecting anatomical images to identify landmarks as they are not easily seen in the lower-resolution BOLD (functional) images. The use of anatomical landmarks is necessary for the development of a common coordinate system of the placenta. Nevertheless, this work is the first step towards developing a common coordinate system to visualize, examine, and study the organ as well as to support statistical analysis across subjects and time. Such a framework promises to advance the state of the art in studies of the placenta and to provide MRI biomarkers of fetal health.

Acknowledgments

This work was supported in part by NIH NICHD U01HD087211, NIH NIBIB NAC P41EB015902, Wistron Corporation, SIP, AWS, NSF GRFP, AND NSERC PGS D.

References

1. Benirschke, K., Driscoll, S.G.: The pathology of the human placenta. In: *Placenta*, pp. 97–571. Springer Berlin Heidelberg (1967)
2. Fang, Q., Boas, D.A.: Tetrahedral mesh generation from volumetric binary and grayscale images. In: *2009 IEEE International Symposium on Biomedical Imaging: From Nano to Macro*. pp. 1142–1145 (2009)
3. Fischl, B., Sereno, M.I., Dale, A.M.: Cortical surface-based analysis: II: inflation, flattening, and a surface-based coordinate system. *Neuroimage* **9**(2), 195–207 (1999)
4. Floater, M.S.: Mean value coordinates. *Computer Aided Geometric Design* **20**(1), 19–27 (2003)
5. Floater, M.S., Hormann, K.: Surface parameterization: a tutorial and survey. In: *Advances in Multiresolution for Geometric Modelling*. pp. 157–186. Springer Berlin Heidelberg (2005)
6. Joshi, P., Meyer, M., DeRose, T., Green, B., Sanocki, T.: Harmonic coordinates for character articulation. *ACM Trans. Graph.* **26**(3) (2007)
7. Leow, A.D., Yanovsky, I., Chiang, M.C., Lee, A.D., Klunder, A.D., Lu, A., Becker, J.T., et al.: Statistical properties of Jacobian maps and the realization of unbiased large-deformation nonlinear image registration. *IEEE Transactions on Medical Imaging* **26**(6), 822–832 (2007)
8. Lui, L.M., Wang, Y., Chan, T.F., Thompson, P.: Landmark constrained genus zero surface conformal mapping and its application to brain mapping research. *Applied Numerical Mathematics* **57**(5-7), 847–858 (2007)
9. Luo, J., Turk, E.A., Bibbo, C., Gagoski, B., Roberts, D.J., Vangel, M., Tempany-Afdhal, C.M., et al.: In vivo quantification of placental insufficiency by BOLD MRI: a human study. *Scientific Reports* **7**(1), 3713 (2017)

10. Miao, H., Mistelbauer, G., Karimov, A., Alansary, A., Davidson, A., Lloyd, D.F., Damodaram, M., et al.: Placenta maps: in utero placental health assessment of the human fetus. *IEEE Transactions on Visualization and Computer Graphics* **23**(6), 1612–1623 (2017)
11. Ng, A.Y., Jordan, M.I., Weiss, Y.: On spectral clustering: Analysis and an algorithm. In: *Advances in Neural Information Processing Systems*. pp. 849–856 (2002)
12. Rabinovich, M., Poranne, R., Panozzo, D., Sorkine-Hornung, O.: Scalable locally injective mappings. *ACM Trans. Graph.* **36**(4) (2017)
13. Schreiner, J., Asirvatham, A., Praun, E., Hoppe, H.: Inter-surface mapping. *ACM Trans. Graph.* **23**(3), 870–877 (2004)
14. Si, H.: Tetgen, a Delaunay-based quality tetrahedral mesh generator. *ACM Transactions on Mathematical Software (TOMS)* **41**(2), 11:1–11:36 (2015)
15. Slator, P.J., Hutter, J., McCabe, L., Gomes, A.D.S., Price, A.N., Panagiotaki, E., Rutherford, M.A., et al.: Placenta microstructure and microcirculation imaging with diffusion MRI. *Magnetic Resonance in Medicine* **80**(2), 756–766 (2017)
16. Smith, J., Schaefer, S.: Bijective parameterization with free boundaries. *ACM Trans. Graph.* **34**(4), 70:1–70:9 (2015)
17. Sørensen, A., Peters, D., Simonsen, C., Pedersen, M., Stausbøl-Grøn, B., Christiansen, O.B., Lingman, G., et al.: Changes in human fetal oxygenation during maternal hyperoxia as estimated by BOLD MRI. *Prenatal Diagnosis* **33**(2), 141–145 (2013)
18. Timsari, B., Leahy, R.M.: Optimization method for creating semi-isometric flat maps of the cerebral cortex. In: *Proc.SPIE, Medical Imaging: Image Processing*. vol. 3979, pp. 698–709 (2000)
19. Tosun, D., Prince, J.L.: Hemispherical map for the human brain cortex. In: *Proc.SPIE, Medical Imaging: Image Processing*. vol. 4322, pp. 290–301 (2001)